



Alexandria University
Alexandria Engineering Journal

www.elsevier.com/locate/aej
www.sciencedirect.com



ORIGINAL ARTICLE

Entropy generation analysis of MHD hybrid nanofluid flow due to radiation with non-erratic slot-wise mass transfer over a rotating sphere



Tapas Barman^a, S. Roy^{a,*}, Ali J. Chamkha^b

^a Mathematics Department, IIT Madras, Chennai 600036, India

^b Faculty of Engineering, Kuwait College of Science and Technology, Doha District, 35004, Kuwait

Received 1 September 2022; revised 13 December 2022; accepted 21 December 2022

KEYWORDS

Hybrid nanofluid;
 Matrix iterative method;
 Entropy production;
 Temperature-sensorial water properties;
 Non-erratic slot-wise mass disposal

Abstract Flow over rotating spheres has serious applications in fiber coating, rotating machinery design and parts, and projectile missions. Therefore, the current study investigates the flow and entropy generation of a radiative magneto-hybrid nanofluid flow over rotating sphere. Further, the temperature-sensorial water properties in studying water-based nanofluids are ignored, though this erratic behavior of water characteristics influences the physical characteristics of the corresponding hybrid nanofluid. Hence the current framework is one of the foremost projects to introduce the variable nature of water properties in the water-hosted hybrid nanofluid flow analysis. The investigation is accomplished in the account of the modified Buongiorno model (MBM). The flow separation in this kind of flow geometry is controlled by using non-erratic slot-mass transfer. The mathematical representations of the physical principles of the flow are solved using (i) congenial transformation (ii) quasilinearization (iii) methods of finite differences to form a block matrix system, and (iv) Varga's iterative algorithm. Some of the major outcomes are: The flow separation can be significantly delayed using slot suction, precisely appointing them downstream with higher strengths; heat transport performance drastically subsidies for high viscous dissipation (Ec), entropy produces at higher rate for viscous heating (Br) and high angular speed (Ω).

© 2022 THE AUTHORS. Published by Elsevier B.V. on behalf of Faculty of Engineering, Alexandria University. This is an open access article under the CC BY-NC-ND license (<http://creativecommons.org/licenses/by-nc-nd/4.0/>).

1. Introduction:

The study of fluid flow around a rotund sphere received the concentration of several researchers due to its diverse applica-

tions in applied engineering fields like fiber coating, rotating machinery design and parts, projectile missions, etc. In early studies, Kumari and Nath [1,2] studied the thermal transport and flow phenomenon for forced flow over a rotating sphere in both steady and unsteady cases. Then an unsteady flow was investigated in the front side stagnation region of a rotund sphere by Takhar et al. [3]. Roy and Saikrishnan [4] numerically scrutinized temperature-sensorial fluid flow up to the separation point. As an analogous study, they [5] studied the

* Corresponding author.

E-mail address: sjroy@iitm.ac.in (S. Roy).

Peer review under responsibility of Faculty of Engineering, Alexandria University.

<https://doi.org/10.1016/j.aej.2022.12.051>

1110-0168 © 2022 THE AUTHORS. Published by Elsevier B.V. on behalf of Faculty of Engineering, Alexandria University. This is an open access article under the CC BY-NC-ND license (<http://creativecommons.org/licenses/by-nc-nd/4.0/>).

Nomenclature

C_p	Specific heat capacitance ($JK^{-1}kg^{-1}$)
C	Species concentration
D_B, D_T	Diffusions coefficients for Brownian and Thermophoretic, respectively
g	Gravity (ms^{-2})
K	Conductivity (thermal) ($Wm^{-1}K^{-1}$)
q_r	Radiation heat flux
Q_0	Heat sink/source
R^*D	D is the mass diffusivity and R^* is a constant
ρ	Density (kgm^{-3})
σ	Conductivity (electrical)(Sm^{-1})
ϕ	NP volume percentage
ψ	Streamfunction

Non-dimensional functions

f, S	Streamfunction
F, S	Chord-wise and span-wise velocity, respectively
G	Temperature

H	Concentration
-----	---------------

Subscripts

e	Condition at BL edge w, ∞ Conditions at surface, ambient fluid, respectively
hnf	Hybrid NF
f	Fluid
s	Solid NPs
s_1, s_2	Cu and Al_2O_3 nanoparticles

Abbreviations

NF	Nanofluid
NP	Nanoparticle
EG	Entropy generation
BL	Boundary Layer
HNF	Hybrid Nanofluid

effect of non-erratic slot-wise mass transfer and pointed out that the considered method (non-erratic slot-wise mass disposal) can push back the separation point. Turkyilmazoglu [6] derived analytical expressions and numerical solutions of a porous flow for rotating spheres under uniform surface mass disposal and outlying magnetic field effects. On the stagnation region (forward) of a rotund sphere, numerical scrutiny of an MHD casson nanofluid (NF) flow was accomplished by Mahdy et al. [7]. Some other researchers [8,9] also pursued numerical analysis of NF flow over the same geometry. Gul et al. [10] elaborated an investigation on the blood-based hybrid nanofluid (HNF) flow under an outlying magnetic field.

Nanofluid (NF) has already shown great potential in enhancing thermal performance. Since the demands for high thermal performance are very high in the recent era of nano-engineering, the application of NFs is tremendously increasing in various industrial, electrical, biomedicine, and engineering sectors. The following articles [11–14] may help to find the diverse application of NFs. HNF, on the other hand, is a new kind of nano-liquid made up by hybridizing two or more different types of NPs with more extraordinary ability in thermal transport amplification. Due to its incredible potential in heat transportation, a vast number of researchers across the globe have conducted numerous research attempts on HNF flow. In modern fluid technology, hybrid nanofluid (HNF) becomes very essential due to its tremendous performance in heat transportation and it shows better performance in the heat transport means than regular fluid or ordinary NFs. Some important studies regarding this topic are cited here for curious researchers [15–24].

The present study basically initiated with the modified version of nanofluid model proposed by Buongiorno [25]. Buongiorno's model sophisticatedly considers the two major slip mechanisms, diffusion of Brownian and thermophoresis, though it is unable to incorporate the thermo-physical characteristics of nanofluids. The revised version of this model, known as the modified Buongiorno model (MBM) [26–29]

considers the slip mechanisms as well as incorporates the thermo-physical characteristics of nanofluids (hybrid). The physical characteristics of base liquid and nanoparticles, in a way, influence the properties of nanofluid (hybrid); and these connections are presented through different correlations. Hence, the MBM consolidates the essential properties of nano-liquid and the effective slip mechanisms (Brownian and thermophoresis). Mahanthesh et al. [26] employed this revised model to study sensitivity analysis of hybrid nanofluid for a wedge. Puneeth and others [27] investigated hybrid nanofluid flow using MBM in biomedical aspect. Rana et al. [28] investigated 3D flow utilizing MBM over a two dimensional extended surface. Owhaib et al. [29] studied 3D dissipating (viscous), radiative nanofluid flow considering MBM. Also, researchers [30] studied hybrid casson nanofluid flow using MBM over a bi-directional elongated sheet (non-linear).

Several researchers have investigated the impact of radiation and MHD on HNF flow. A magnetic field outlying magnetic nanoparticles (NPs) boundary layer (BL) flow has a vast area of applications, like MHD-generators, MHD-pumps, MHD-motor, drug delivery, etc. Even it can be used to form desired structures in material processing [31]. Alghamdi et al. [32] have studied blood-based HNF flow, in which they notified that radiation and MHD play a major role in the flow. Anantha Kumar et al. [33] deliberated a note on radiative MHD ferrofluid flow (hybrid) for a thin film. Othman et al. [34] scrutinized the MHD and radiation impacts on CNT-based HNF flow along a shrinking porous surface. Shoaib and others [35] numerically scrutinized radiative MHD 3-D flow utilizing the method of Lobatto IIIA. Also, similar recent studies on this topic may be referred here [36–42].

For the shake of better perfection in any thermo-dynamical system, it is necessary to track the irreversible heat losses so that the system can be made more effective by reducing the undesired heat losses. Entropy generation (EG) is the best way to monitor such irreversibilities. So, the authors of this existing project not only scrutinized the flow phenomena and

heat transport but also performed an enumeration of generated entropy in the system. Khan et al. [43] focused on the EG study of water – *Go* – *Cu* HNF flow in a rotating system with MHD, radiation, and chemical reaction effects. Qureshi et al. [44] presented a comprehensive EG analysis of a time-dependent HNF flow for MHD, Joule heating, viscous dissipation, etc. effects over parallel/coaxial plates. Li and others [45] discussed the entropy nature of an HNF flow for a disk affected by radiation, dissipation (viscous), thermal sink-source, and bi-convection. In this aspect, the following cited texts may be found informative [46–51].

2. Motivation

In theories as well as in experiments, water-hosted NF/HNF has been found as temperature-sensitive. Also, the physical attributes of NPs and base liquid are consolidated in the thermos-physical characteristics of HNFs. Hence, it is well expected to incorporate the host liquid's properties in the HNF study. But in common practice, these facts are being ignored, and even sometimes constant water (host liquid) properties are being considered. In fact, this study is primarily focused on a forced convective HNF flow taking the temperature-sensorial water properties (physical) into account. The changing natures of a few basic thermos-physical water attributes via temperature variation/modification are modeled [4] using empirical data [52]. Further, the flow is considered over a complex geometric spinning sphere which has numerous practical implementations in engineering. The point of separation which occurs due to adverse pressure gradient within the BL flow region is controlled via slot-wise mass disposal method. The boundary layer (BL) flow of electrically conducting HNFs are assumed to flow under an outlying magnetic field along with external radiation effects. Further, this existing project is accomplished with the modified Buongiorno model (MBM), the foremost advanced method available in literature. The governing PDEs (non-linear and coupled) have been solved employing sets of advanced numerical methods that comprised quasilinearization, finite difference (implicit), Vargas method [53]. The results are comprehensively illustrated in graphical formats for better discernment to understand the complex results.

3. Models and correlations:

The empirical data set given in Table 1 that shows the transitional behaviour of water properties in temperature changes are modeled as [54]

$$\mu_f(T) = \frac{1}{b_1 + b_2 T} \quad (1)$$

$$(Pr)_f(T) = \frac{1}{c_1 + c_2 T} \quad (2)$$

with

$$\begin{pmatrix} b_1 \\ b_2 \\ c_1 \\ c_2 \end{pmatrix} = \begin{pmatrix} 53.41 \\ 2.43 \\ 0.068 \\ 0.004 \end{pmatrix}$$

The correlations between physical characteristics of HNF with that of host liquid (water) and NPs [55] are

$$\mu_{hmf}(T, \phi) = (1 - \phi)^{-2.5} \mu_f(T); \phi = \phi_{s_1} + \phi_{s_2} \quad (3)$$

$$\rho_{hmf}(T, \phi) = [(1 - \phi)\rho_f(T) + \rho_{s_1}\phi_{s_1} + \rho_{s_2}\phi_{s_2}] \quad (4)$$

$$(C_p\rho)_{hmf}(T, \phi) = [(1 - \phi)(C_p\rho)_f(T) + (C_p\rho)_{s_1}\phi_{s_1} + (C_p\rho)_{s_2}\phi_{s_2}] \quad (5)$$

$$\begin{aligned} \sigma_{hmf}(T, \phi) &= \sigma_f(T) \left[1 + \frac{3\phi(\Psi_1 - \phi\sigma_f)}{\Psi_2 - (\Psi_1 - \phi\sigma_f)\phi} \right]; \Psi_1 \\ &= (\sigma\phi)_{s_1} + (\sigma\phi)_{s_2}; \Psi_2 = \Psi_1 + 2\phi\sigma_f \end{aligned} \quad (6)$$

$$\begin{aligned} k_{hmf}(T, \phi) &= \left[\frac{2k_f(T) + \frac{\Psi_3}{\phi} - 2(\phi k_f(T) - \Psi_3)}{2k_f(T) + \phi k_f(T) + \left(\frac{\Psi_3}{\phi} - \Psi_3\right)} \right] k_f(T); \Psi_3 \\ &= (\phi k)_{s_1} + (\phi k)_{s_2} \end{aligned} \quad (7)$$

As evidenced in Table 1, water density ρ_f , and specific heat $(C_p)_f$ show significantly less variation ($< 1\%$) and so, they can be treated as constant properties. Likewise, it can be shown that the variations of those properties (ρ_{hmf} and $(C_p)_{hmf}$) for water-hosted HNF are also very less ($< 1\%$) [56]. Hence, for the water-hosted HNF study, they can be considered unaltered in temperature. In addition, the properties of solid NPs (*Cu*, *Al₂O₃*) are stable in the considered moderate temperature range $10^\circ\text{C} - 50^\circ\text{C}$ and one might treat them as constant (Table 2.).

4. Governing equations:

An incompressible hybrid NF forced convective flow with temperature-sensorial base-fluid characteristics, over a rotating sphere of radius R is considered where the sphere is revol-

Table 1 Water properties vs temperatures [52].

T (C)	ρ (g . cm ⁻³)	C_p (J.10 ⁷ .kg ⁻¹ K ⁻¹)	k (erg. 10 ⁵ .cm ⁻¹ .s ⁻¹ . K ⁻¹)	μ (g. 10 ⁻² .cm ⁻¹ .s ⁻¹)	Pr
0	1.00228	4.2176	0.5610	1.7930	13.4
10	0.99970	4.1921	0.5800	1.3070	9.45
20	0.99821	4.1818	0.5984	1.0060	7.03
30	0.99565	4.1784	0.6154	0.7977	5.12
40	0.99222	4.1785	0.6305	0.6532	4.32
50	0.98803	4.1806	0.6435	0.5470	3.55

Table 2 Nanoparticle properties [56,57].

Properties	Copper	Alumina
$C_p(Jkg^{-1}K^{-1})$	385	765
$\rho(kg.m^{-3})$	8933	3970
$k(Wm^{-1}K^{-1})$	400	40
$\beta \times 10^{-5}K^{-1}$	1.67	0.85

ing perpendicular to the ambient flow direction. A curvilinear (orthogonal) system of axes is considered where (see Fig. 1):

- (i) The chord-wise distance from the forward stagnation point along a meridian is measured by x
- (ii) The distance in span-wise direction, i.e., in the direction of rotation is measured by y
- (iii) The normal distance from the sphere surface perpendicular to x and y axes is measured by z

The radius of a section perpendicular to the sphere's axis at a distance x along a meridian measured from the centre is considered as $r(x)$ and it is also assumed that the corresponding BL thickness is less enough compared to $r(x)$. The electrically conducted HNF flow is flowing under the influence of an outlying magnetic field (B_0) and external radiation (q_r) in moderate temperature deviation ($< 40^\circ C$). The effects of slot-wise mass disposal and viscous dissipation are also included in this analysis. The fluid at the BL edge wall is assumed to maintain a constant temperature T_∞ and the bounding surface is assumed to be uniform temperature $T_w(T_w > T_\infty)$. The

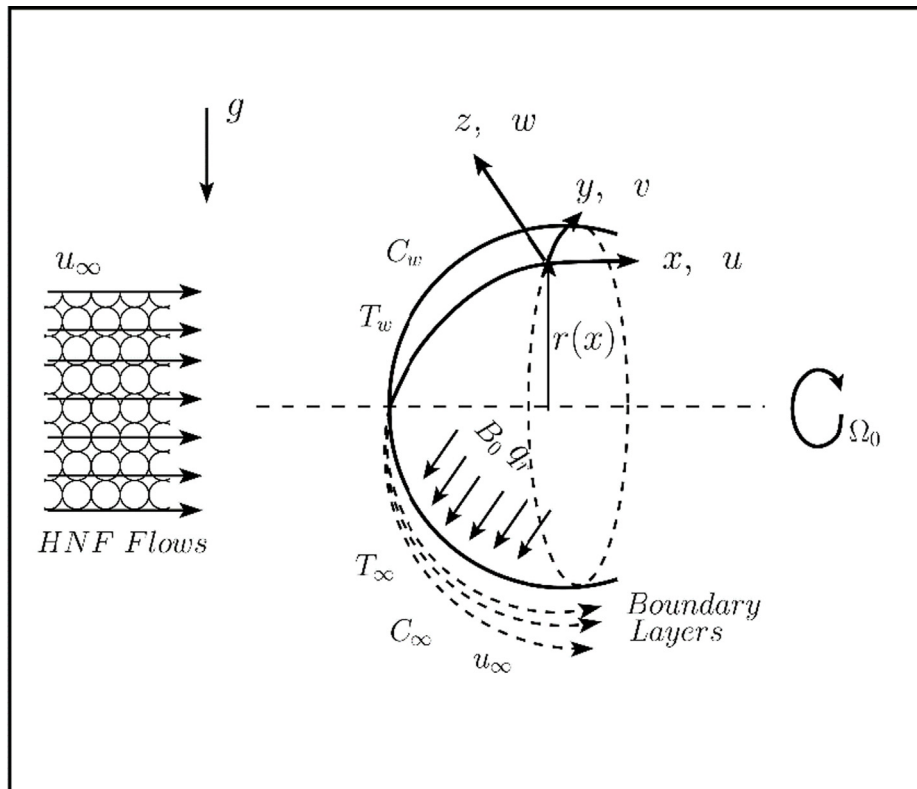
slot-wise blow at the wall is assumed to be small enough that it does not affect the freestream flow at the BL edge. Additionally, it is assumed that the injected fluid has the same physical characteristics as BL fluid and that its static temperature is equivalent to that of the wall. Some of the physical characteristics like density, specific heat of the HNF are considered as constant while the rest are considered as temperature sensorial. Under these assumptions, the governing BL equations for an HNF flow over a rotund sphere in modified Buongiorno model (MBM) are [4,27]:

$$\frac{\partial(ru)}{\partial x} + \frac{\partial(rw)}{\partial z} = 0 \quad (8)$$

$$u \frac{\partial u}{\partial x} + w \frac{\partial u}{\partial z} - \frac{v^2}{r} \frac{dr}{dx} = u_e \frac{du_e}{dx} + \frac{1}{\rho_{hmf}} \frac{\partial}{\partial z} \left(\mu_{hmf} \frac{\partial u}{\partial z} \right) - \frac{\sigma_{hmf} B_0^2}{\rho_{hmf}} \times (u - u_e) \quad (9)$$

$$u \frac{\partial v}{\partial x} + w \frac{\partial v}{\partial z} + \frac{uv}{r} \frac{dr}{dx} = \frac{1}{\rho_{hmf}} \frac{\partial}{\partial z} \left(\mu_{hmf} \frac{\partial v}{\partial z} \right) - \frac{\sigma_{hmf} B_0^2}{\rho_{hmf}} v \quad (10)$$

$$u \frac{\partial T}{\partial x} + w \frac{\partial T}{\partial z} = \frac{1}{(\rho C_p)_{hmf}} \frac{\partial}{\partial z} \left(k_{hmf} \frac{\partial T}{\partial z} \right) + \frac{(C_p \rho)_s}{(C_p \rho)_{hmf}} \left[D_B \frac{\partial C}{\partial z} \frac{\partial T}{\partial z} + \frac{D_T}{T_\infty} \left(\frac{\partial T}{\partial z} \right)^2 \right] + \frac{(\mu)_{hmf}}{(C_p \rho)_{hmf}} \left[\left(\frac{\partial u}{\partial z} \right)^2 + \left(\frac{\partial w}{\partial z} \right)^2 \right] - \frac{1}{(\rho C_p)_{hmf}} \frac{\partial q_r}{\partial z} \quad (11)$$

**Fig. 1** Flow geometry.

$$u \frac{\partial C}{\partial x} + w \frac{\partial C}{\partial z} = D_B \frac{\partial^2 C}{\partial z^2} + \frac{D_T}{T_\infty} \frac{\partial^2 T}{\partial z^2} \tag{12}$$

where

$$(C_p \rho)_s = \frac{\phi_{s1} (C_p \rho)_{s1} + \phi_{s2} (C_p \rho)_{s2}}{\phi_{s1} + \phi_{s2}}$$

$$\text{and } q_r = -\frac{4\sigma^*}{3k^*} \frac{\partial T^4}{\partial z}$$

The constraints at the boundaries are given by:

$$C = C_w; T = T_w; u = 0, v = \Omega_0 r(x); w = w_w(x); \text{ at } z = 0 \tag{13}$$

$$C \rightarrow C_\infty; T \rightarrow T_\infty; u \rightarrow u_e; v = 0; w = 0; \text{ as } z \rightarrow \infty \tag{14}$$

The Eqs. (9)–(12) are transformed into simplified versions appointing the following congenial coordinate changes:

$$\xi = \int_0^x \left(\frac{u_e}{u_\infty}\right) \left(\frac{r}{R}\right)^2 d\left(\frac{x}{R}\right); \eta = \sqrt{\left(\frac{Re}{2\xi}\right)} \left(\frac{u_e}{u_\infty}\right) \left(\frac{r}{R}\right) \left(\frac{z}{R}\right)$$

$$\psi = u_\infty R \sqrt{\left(\frac{2\xi}{Re}\right)} f(\xi, \eta); R \frac{\partial \psi}{\partial x} = -wr; R \frac{\partial \psi}{\partial z} = ru;$$

$$f_\eta = F; v = \Omega_0 r(x) S(\xi, \eta); Re = \frac{u_\infty R}{\nu_\infty}$$

$$G = \frac{T - T_w}{T_\infty - T_w} = \frac{T - T_w}{-\Delta T}, \Delta T = T_w - T_\infty (T_w > T_\infty);$$

$$H = \frac{C - C_\infty}{\Delta C}, \Delta C = C_w - C_\infty (C_w > C_\infty)$$

The simplified form of Eqs. (9)–(12) after transformation turned into:

$$\begin{aligned} &\frac{\partial}{\partial \eta} \{NF_\eta\} \\ &+ S_1 [(1 - F^2)m + fF_\eta - 2\xi (FF_\xi - f_\xi F_\eta) + \Omega n S^2] \\ &- 2\xi K_1 St (F - 1) \left(\frac{u_\infty R}{u_e r}\right)^2 \\ &= 0 \end{aligned} \tag{15}$$

$$\begin{aligned} &\frac{\partial}{\partial \eta} \{NS_\eta\} + S_1 [fS_\eta - 2nFS - 2\xi (FS_\xi - f_\xi S_\eta)] \\ &- 2\xi K_1 St S \left(\frac{u_\infty R}{u_e r}\right)^2 \\ &= 0 \end{aligned} \tag{16}$$

$$\begin{aligned} &\left[\frac{N}{Pr} (P_5 + R_1)\right] G_{\eta\eta} + G_\eta \frac{\partial}{\partial \eta} \left(\frac{N}{Pr} P_5\right) \\ &+ \frac{EcN}{\sqrt{(1 - \phi)^5}} [F_\eta^2 + \Omega S_\eta^2] \left(\frac{u_e}{u_\infty}\right)^2 + [NbH_\eta + NtG_\eta] G_\eta \\ &+ S_2 [fG_\eta - 2\xi (FG_\xi - f_\xi G_\eta)] \\ &= 0 \end{aligned} \tag{17}$$

$$H_{\eta\eta} + \frac{Nt}{Nb} G_{\eta\eta} + Sc [fH_\eta - 2\xi (FH_\xi - f_\xi H_\eta)] = 0 \tag{18}$$

with the constraints

$$\begin{bmatrix} F \\ S \\ G \\ H \end{bmatrix}_{\eta=0} = \begin{bmatrix} 0 \\ 1 \\ 0 \\ 1 \end{bmatrix}; \begin{bmatrix} F \\ S \\ G \\ H \end{bmatrix}_{\eta=\eta_\infty} = \begin{bmatrix} 1 \\ 0 \\ 1 \\ 0 \end{bmatrix} \tag{19}$$

Here the parameters of rotation, radiation, Eckert number, Brownian motion, Thermophoresis, and Schmidt number are defined respectively as:

$$\Omega = \left(\frac{\Omega_0 r}{u_e}\right)^2; R_1 = \frac{16\sigma^* T_\infty^3}{3k^* k_f}; Ec = -\frac{U_\infty^2}{C_p \Delta T}; Nb = \tau \frac{D_B \Delta C}{\nu_\infty};$$

$$Nt = -\tau \frac{D_T \Delta T}{\nu_\infty T_\infty}; Sc = \frac{\nu_\infty}{D_B} \text{ where } \tau = \frac{(C_p \rho)_s}{(C_p \rho)_f}$$

The other coefficients are defined as:

$$m = \frac{2\xi}{u_e} \frac{du_e}{d\xi}; n = \frac{2\xi}{r} \frac{dr}{d\xi}; N = \frac{1}{1 + a_1 G}, Pr = \frac{1}{d_1 + d_2 G}$$

$$\begin{aligned} a_1 &= \frac{-b_2 \Delta T}{b_1 + b_2 T_\infty}, a_2 = b_1 + b_2 T_\infty, a_3 = a_1 a_2, d_1 \\ &= c_1 + c_2 T_\infty, d_2 = -c_2 \Delta T \end{aligned}$$

$$P_1 = a_2 \Psi_3 (1 + 2\phi) + 2\phi (C_p)_f d_1 (1 - \phi)$$

$$P_2 = a_3 \Psi_3 (1 + 2\phi) + 2\phi (C_p)_f d_2 (1 - \phi)$$

$$P_3 = (1 - \phi) a_2 \Psi_3 + (2 + \phi) \phi (C_p)_f d_1;$$

$$P_4 = (1 - \phi) a_3 \Psi_3 + (2 + \phi) \phi (C_p)_f d_2$$

$$P_5 = \frac{P_1 + P_2 G}{P_3 + P_4 G}, P_6 = \frac{d_2 - a_1 d_1}{(1 + a_1 G)^2}, P_7 = \frac{P_2 P_3 - P_1 P_4}{(P_3 + P_4 G)^2},$$

$$P_8 = -a_1 \frac{(d_2 - a_1 d_1)}{(1 + a_1 G)^3}, P_9 = -P_4 \frac{(P_2 P_3 - P_1 P_4)}{(P_3 + P_4 G)^3}$$

$$S_1 = \left\{ 1 - \left(1 - \frac{(\rho)_{s_1}}{(\rho)_f} \right) \phi_{s_1} - \left(1 - \frac{(\rho)_{s_2}}{(\rho)_f} \right) \phi_{s_2} \right\} \sqrt{(1 - \phi)^5},$$

$$S_2 = \left\{ 1 - \left(1 - \frac{(C_p \rho)_{s_1}}{(C_p \rho)_s} \right) \phi_{s_1} - \left(1 - \frac{(C_p \rho)_{s_2}}{(C_p \rho)_s} \right) \phi_{s_2} \right\}$$

Here $f = \int_0^\eta F d\eta + f_w$ where $f_w = -\sqrt{\frac{Re}{2\xi}} \int_0^{\bar{x}} \left(\frac{r}{R}\right) \frac{w_w(\bar{x})}{u_\infty} d\bar{x}$.

The set of Eqs. (15)-(18) reduces to that of the classical non-similar flow over a stationary sphere for $\Omega = 0$ and $\phi = 0$.

The free stream velocity at the BL edge and the radius of revolution $r(x)$ are given by [58]

$$\frac{u_e}{u_\infty} = \frac{3}{2} \sin \bar{x}, \frac{r}{R} = \sin \bar{x}, \text{ where } \bar{x} = \frac{x}{R}$$

Using these relations, the Eqs. (15)–(18) turned into:

$$\frac{\partial}{\partial \eta} \{NF_\eta\} + S_1 \left[\frac{T_3 T_4}{T_2} ((1 - F^2) + \Omega S^2) + fF_\eta - 2 \frac{T_3 T_5}{T_2} (FF_{x^-} - f_{x^-} F_\eta) \right] - \frac{4}{9} \frac{T_3}{T_2} K_1 St (F - 1) = 0 \tag{20}$$

$$\frac{\partial}{\partial \eta} \{NS_\eta\} + S_1 \left[fS_\eta - 2 \frac{T_3 T_4}{T_2} FS - 2 \frac{T_3 T_5}{T_2} (FS_{x^-} - f_{x^-} S_\eta) \right] - \frac{4}{9} \times \frac{T_3}{T_2} \xi K_1 St S = 0 \tag{21}$$

$$\left[\frac{N}{Pr} (P_5 + R_1) \right] G_{\eta\eta} + G_\eta \frac{\partial}{\partial \eta} \left(\frac{N}{Pr} P_5 \right) + \frac{9}{4} \times \frac{EcNT_1 T_2}{\sqrt{(1 - \phi)^5}} \left[F_\eta^2 + \Omega S_\eta^2 \right] + [NbH_\eta + NtG_\eta] G_\eta + S_2 \left[fG_\eta - 2 \frac{T_3 T_5}{T_2} (FG_{x^-} - f_{x^-} G_\eta) \right] = 0 \tag{22}$$

$$H_{\eta\eta} + \frac{Nt}{Nb} G_{\eta\eta} + Sc \left[fH_\eta - 2 \frac{T_3 T_5}{T_2} (FH_{x^-} - f_{x^-} H_\eta) \right] = 0 \tag{23}$$

with the boundary constraints same as (19).

Here $T_1 = (1 - \cos \bar{x})$; $T_2 = (1 + \cos \bar{x})$; $T_3 = (2 + \cos \bar{x})$; $T_4 = \frac{2}{3} \cos \bar{x}$; $T_5 = \frac{1}{3} \tan \left(\frac{\bar{x}}{2} \right)$ and the expressions for ξ, m, n and f_w are changed into $\xi = \frac{1}{2} T_1^2 T_3$; $m = \frac{T_3 T_4}{T_2^2}$, $n = \frac{T_3 T_4}{T_2^2} \xi \frac{\partial}{\partial \xi} = \frac{T_3 T_5}{T_2} \frac{\partial}{\partial x}$ and

$$f_w = \begin{cases} 0 & \bar{x} \leq \bar{x}_1 \\ \frac{A}{T_1 \sqrt{T_3}} C(\bar{x}, \bar{x}_1) & \bar{x} \in [\bar{x}_1, \bar{x}_2] \\ \frac{A}{T_1 \sqrt{T_3}} C(\bar{x}_2, \bar{x}_1) & \bar{x} \geq \bar{x}_2 \end{cases}$$

$$\text{with } C(\bar{x}, \bar{x}_1) = \frac{\sin[(2\pi-1)\bar{x} - 2\pi\bar{x}_1] + \sin[\bar{x}_1]}{(2\pi-1)} - \frac{\sin[(2\pi+1)\bar{x} - 2\pi\bar{x}_1] + \sin[\bar{x}_1]}{(2\pi+1)}$$

The non-erratic slot-wise mass transfer function $w_w(\bar{x})$ is considered as:

$$w_w(\bar{x}) = \begin{cases} 0 & \bar{x} \leq \bar{x}_1 \\ \frac{2u_\infty}{\sqrt{Re}} A \sin [2\pi(\bar{x} - \bar{x}_1)] & \bar{x} \in [\bar{x}_1, \bar{x}_2] \\ 0 & \bar{x} \geq \bar{x}_2 \end{cases}$$

where $[\bar{x}_1, \bar{x}_2]$ represent the slot and A defines the slot strength.

The friction coefficients in x and y directions are:

$$C_{f_1} = \frac{2\mu_{mf} \left(\frac{\partial u}{\partial z} \right)_w}{\rho_{mf} u_\infty^2}, C_{f_2} = \frac{2\mu_{mf} \left(\frac{\partial v}{\partial z} \right)_w}{\rho_{mf} U_\infty^2}$$

and after coordinate transformations, they become

$$\sqrt{Re} C_{f_1} = 4.5 \sqrt{T_1 T_2} \frac{T_2}{\sqrt{T_3}} \frac{(N)_w}{S_1} (F_\eta)_w \text{ and } \sqrt{Re} C_{f_2} = 4.5 \sqrt{T_1 T_2} \frac{T_2 \Omega}{\sqrt{T_3}} \frac{(N)_w}{S_1} (S_\eta)_w.$$

Similarly, the transport coefficients

$$Nu = \frac{Rq_w}{k_f \Delta T} \left[\text{where } q_w = -k_{mf} \left(\frac{\partial T}{\partial z} \right)_w \right] \text{ and } Sh = \frac{Rq_m}{D_B \Delta C} \left[\text{where } q_m = -D_B \left(\frac{\partial C}{\partial z} \right)_w \right]$$

after transformation become:

$$\frac{Nu}{\sqrt{Re}} = \frac{3}{2} \frac{T_2}{\sqrt{T_3}} (G_\eta)_w \text{ and } \frac{Sh}{\sqrt{Re}} = \frac{3}{2} \frac{T_2}{\sqrt{T_3}} (H_\eta)_w$$

5. Entropy production

The disorder develops in thermodynamical systems in such a way that the system's total available energy is conserved. The available energy in the system of diverse technical and industrial operations is destroyed through entropy creation. Therefore, estimating the system's rate of entropy creation is crucial. The irreversibilities in the considered system are caused by the magnetic field, heat conduction, diffusion, and viscous dissipation. The expression for entropy production in this system may be described as below:

$$S_{gen} = \frac{1}{T_\infty} \underbrace{\left(k_{mf} \left(\frac{\partial T}{\partial z} \right)^2 + \frac{16\sigma^* T_\infty^3}{3k^*} \left(\frac{\partial T}{\partial z} \right)^2 \right)}_{HTI} + \underbrace{\frac{\mu_{mf}}{T_\infty} \left[\left(\frac{\partial u}{\partial z} \right)^2 + \left(\frac{\partial v}{\partial z} \right)^2 \right]}_{FFI} + \underbrace{\frac{R^* D}{T_\infty} \frac{\partial C}{\partial z} \frac{\partial T}{\partial z} + \frac{R^* D}{C_\infty} \left(\frac{\partial C}{\partial z} \right)^2}_{DI}$$

The degree of disorder i.e., entropy primarily generates in three different ways, due to heat transfer (HTI), fluid friction (FFI), and diffusion (DI). The local non-dimensional entropy rate is

$$S_G = \frac{S_{gen}}{S_0} = N_1 + N_2 + N_3$$

where S_0 is the characteristics entropy rate interpreted as

$$S_0 = \frac{\Delta T^2 k_f}{L^2 T_\infty}$$

$$N_1 = \frac{HTI}{S_0} = \left(\frac{9}{4}\right) [P_5 + R_1] Re \left(\frac{T_2^2}{T_3}\right) G_\eta^2$$

$$N_2 = \frac{FFI}{S_0} = \left(\frac{3}{2}\right)^4 \left(\frac{N}{\sqrt{(1-\phi)^5}}\right) \left(\frac{T_1 T_2^3}{\alpha_1 T_3}\right) [F_\eta^2 + \Omega S_\eta^2] Re Br$$

$$N_3 = \frac{DI}{S_0} = \left(\frac{9}{4}\right) \left(\frac{T_2^2}{T_3}\right) \left(\frac{\alpha_3}{\alpha_1}\right) \left[\left(\frac{\alpha_2}{\alpha_1}\right) H_\eta + G_\eta\right] Re H_\eta$$

and the $\alpha_1 = -\frac{\Delta T}{T_\infty}$, $\alpha_2 = \frac{\Delta C}{C_\infty}$, $\alpha_3 = \frac{R^* DC_\infty}{k_f}$ and $Br = \frac{\mu_\infty u_\infty^2}{k_f \Delta T}$ are specified as temperature ratio, concentration ratio, diffusion variable and Brinkman number. The Bejan number (Be) is evaluated as

$$Be = \frac{HTI}{HTI + FFI + DI} = \frac{N_1}{N_1 + N_2 + N_3}$$

= $\frac{\text{Irreversibilities due to heat transfer}}{\text{Total local entropy}}$

6. Numerical approaches

The transformed Eqs. (20)–(23) (non-linear and coupled) are solved utilizing a set of advanced numerical methods that comprised quasi-linearization, finite difference (implicit), Vargas method [38]. The quasi-linearization modified the Eqs. (20)–(23) into the following form:

$$D_{11}^{(k)} F_\eta^{(k+1)} + D_{12}^{(k)} F_\eta^{(k+1)} + D_{13}^{(k)} F_{x^-}^{(k+1)} + D_{14}^{(k)} F^{(k+1)} + D_{15}^{(k)} G_\eta^{(k+1)} + D_{16}^{(k)} G^{(k+1)} + D_{17}^{(k)} S^{(k+1)} = D_{18}^{(k)} \quad (24)$$

$$D_{21}^{(k)} S_\eta^{(k+1)} + D_{22}^{(k)} S_\eta^{(k+1)} + D_{23}^{(k)} S_{x^-}^{(k+1)} + D_{24}^{(k)} S^{(k+1)} + D_{25}^{(k)} F^{(k+1)} + D_{26}^{(k)} G_\eta^{(k+1)} + D_{27}^{(k)} G^{(k+1)} = D_{28}^{(k)} \quad (25)$$

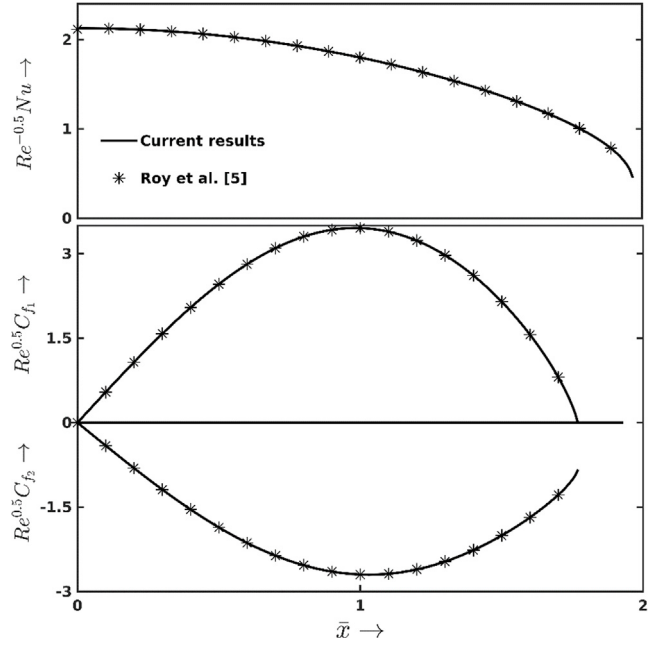


Fig. 2 Results verification.

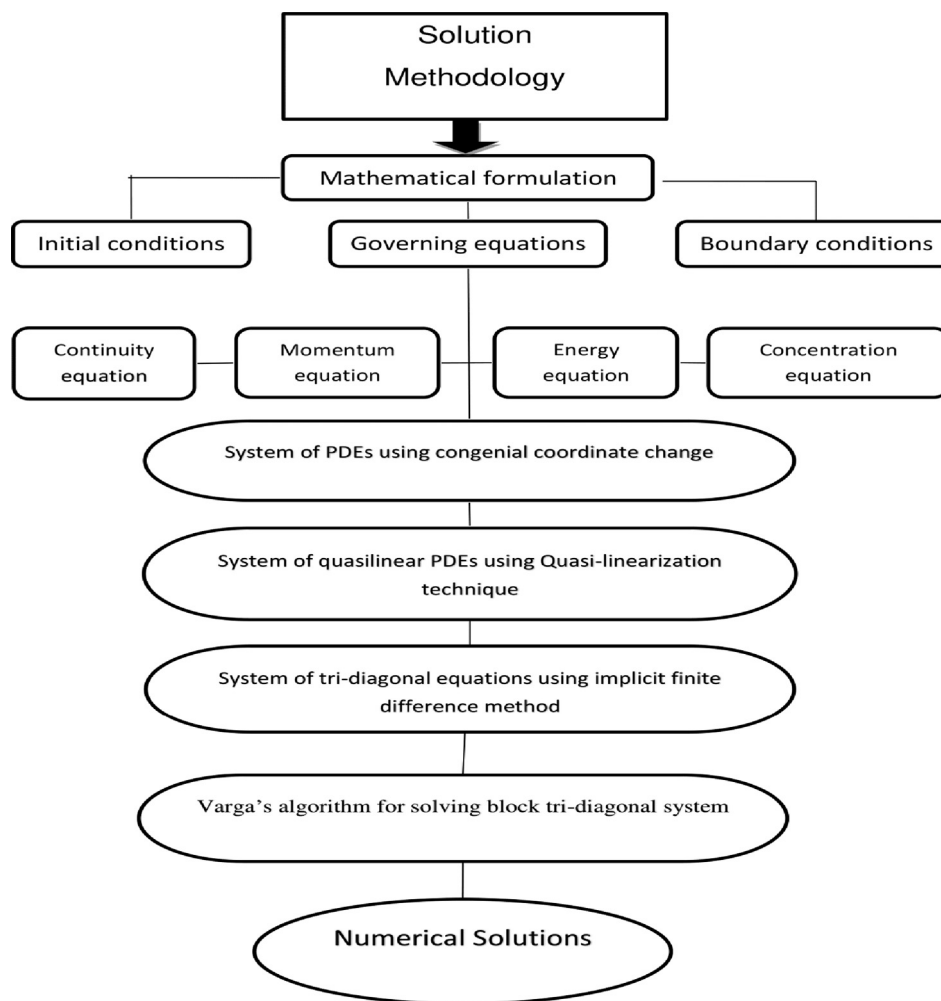
$$D_{31}^{(k)} G_\eta^{(k+1)} + D_{32}^{(k)} G_\eta^{(k+1)} + D_{33}^{(k)} G_{x^-}^{(k+1)} + D_{34}^{(k)} G^{(k+1)} + D_{35}^{(k)} F_\eta^{(k+1)} + D_{36}^{(k)} F^{(k+1)} + D_{37}^{(k)} S_\eta^{(k+1)} + D_{38}^{(k)} H_\eta^{(k+1)} = D_{39}^{(k)} \quad (26)$$

$$D_{41}^{(k)} H_\eta^{(k+1)} + D_{42}^{(k)} H_\eta^{(k+1)} + D_{43}^{(k)} H_{x^-}^{(k+1)} + D_{44}^{(k)} G_\eta^{(k+1)} + D_{45}^{(k)} F^{(k+1)} = D_{46}^{(k)} \quad (27)$$

and

$$\begin{bmatrix} F^{(k+1)} \\ S^{(k+1)} \\ G^{(k+1)} \\ H^{(k+1)} \end{bmatrix}_{\eta=0} = \begin{bmatrix} 0 \\ 1 \\ 0 \\ 1 \end{bmatrix}; \begin{bmatrix} F^{(k+1)} \\ S^{(k+1)} \\ G^{(k+1)} \\ H^{(k+1)} \end{bmatrix}_{\eta=\eta_\infty} = \begin{bmatrix} 1 \\ 0 \\ 1 \\ 0 \end{bmatrix} \quad (28)$$

The Eqs. (24)–(27) represents a linear system with superscript indices $(k+1)$ where $D_{11}, D_{12}, D_{13}, D_{14}, D_{15}, D_{16}, D_{17}, D_{18}; D_{21}, D_{22}, D_{23}, D_{24}, D_{25}, D_{26}, D_{27}; D_{28}, D_{31}, D_{32}, D_{33}, D_{34}, D_{35}, D_{36}, D_{37}, D_{38}, D_{39}; D_{41}, D_{42}, D_{43}, D_{44}, D_{45}, D_{46}$ are prescribed in Appendix. The consequent step of employed numerical tasks i.e., the implicit difference method (finite) reshaped the equations into a block tri-diagonal matrix system that is further solved using Vargas' method. The whole procedure (numerical) is accomplished under a rigorous restriction of convergence conditions and the accurateness of the procedure is illustrated in Fig. 2.



7. Results and discussion

The investigation of EG analysis, flow features and thermal transport for a radiative MHD HNF flow over a rotund sphere in light of temperature-sensorial water properties with non-erratic slot mass disposal is accomplished in this manuscript considering $Cu + Al_2O_3$ /water HNF as working fluid. The obtained results are featured out graphically and discussed in details.

Figs. 3 and 4 are plotted to manifest the variable behaviours of the flow intensities $F(\bar{x}, \eta)$, $S(\bar{x}, \eta)$ against the rotation parameter Ω and magnetic parameter St , respectively. As depicted in Fig. 3, the F -profile rises with Ω while the S -profile deteriorates with Ω . The parameter Ω is present in the momentum equation in the stream-wise direction and an increment in it directly affects the momentum in the stream-wise direction. Hence stream-wise velocity component (F) increases and consequently, the crosswise velocity component (S) decreases. The characterization of velocity components $F(\bar{x}, \eta)$ and $S(\bar{x}, \eta)$ affected by St , the magnetic strength, is portrayed in Fig. 4 which indicates that $S(\bar{x}, \eta)$ gets deteriorated whereas $F(\bar{x}, \eta)$ increases significantly for St . In particular at $\eta = 1.0$, $\bar{x} = 1.5$, in the variation of St from 0 to 1, the increas-

ing and decreasing fluctuations of $F(\bar{x}, \eta)$ and $S(\bar{x}, \eta)$ are, respectively, 14% and 40%. Besides, the effect of Ω and St on non-dimensional stream function are drawn to predict the impact on streamlines (Fig. 5). It is noticed that the magnitude of stream function, i.e., the flow intensity is enhanced due to the increase of both the rotation parameter Ω and magnetic parameter St . Also, the increase in the magnitude of stream function is visible in the region far from the wall.

Fig. 6 depicts the changes in temperature profile $G(\bar{x}, \eta)$ against the dissipation (viscous) and diffusion (thermophoretic) parameters (Ec, Nt) concurrently. It can be simply observed that $G(\bar{x}, \eta)$ enhances for enhancing values of Nt and $|Ec|$. A high dissipative force (large magnitude of $|Ec|$) generates an abundant amount of heat energy owing to viscous friction for HNFs within the BL. Even for higher $|Ec|$ the HNFs near the wall proximity become hotter than the wall, as signified in Fig. 6. In such cases, the wall becomes hotter exploiting heat from the surrounding fluids rather than being cooled down, leading to thermal undershoot near the wall within BL. Further, thermophoresis (Nt) impels the hotter NPs to travel towards the cooler region of the fluid, and this way, the NPs from the hotter surface proximity migrate towards the BL edge, the cooler region. Consequently, the entire BL region gets enriched by temperature.

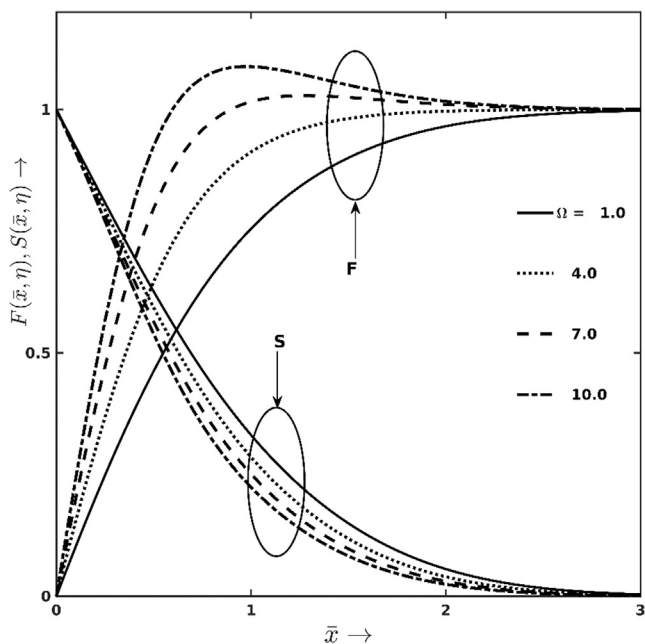


Fig. 3 F and S variation vs. Ω .

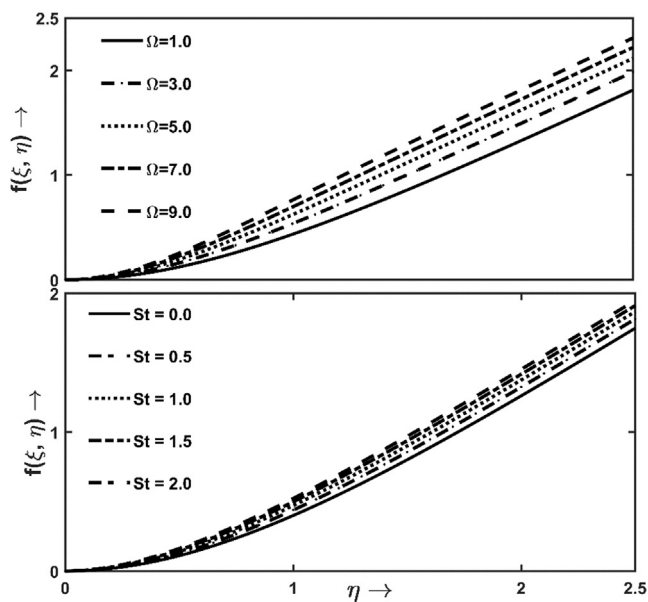


Fig. 5 Ω and St variation on f .

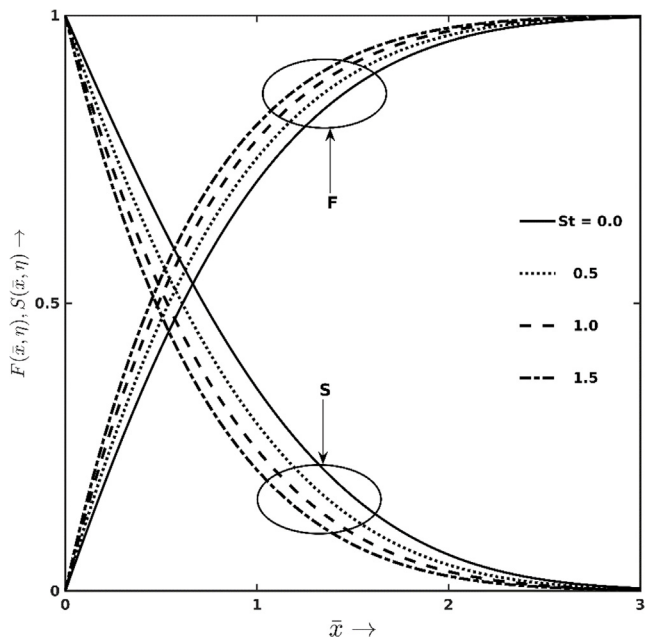


Fig. 4 F and S variation vs. St .

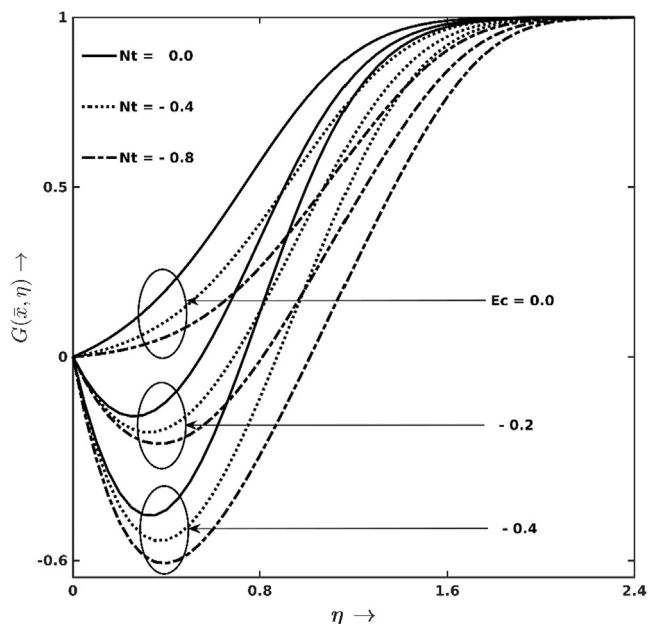


Fig. 6 Ec and Nt variation against G .

The simultaneous effects of the parameters Nb and Sc (Brownian and Schmidt number) on the concentration profile ($H(\bar{x}, \eta)$) is demonstrated in Fig. 7. Close observation on this portrayal discloses that the H -profile declines for both the parameters Nb and Sc . A higher estimation of Sc leads the dominance of momentum diffusion over mass diffusion. On other words, the fluids within BL moves faster and results thinner BL. In addition, high magnitude of Nb intensify NPs' haphazard motion and frequent collision among them, resulting mass equilibrium in the BL region. Hence, in both the cases, H -profile shrinks. The numerical evidences reveal that the H -

profile drops down nearly by 30% for heightening Sc from magnitude 0.7 to 2.57 at $\eta = 0.7$ with fixed $Nb = 0.3$.

The variations of both the friction coefficients $\sqrt{Re}C_{f_1}$ (stream-wise) and $\sqrt{Re}C_{f_2}$ (chord-wise) under the changes of St (magnetic strength) and Ω (rotation parameter) are sketched in Fig. 8. A higher revolution rate (i.e., higher Ω) of the sphere is generating more friction in the x direction ($\sqrt{Re}C_{f_1}$) and behaving exactly opposite to the friction coefficient in y direction ($\sqrt{Re}C_{f_2}$) with fixed values of St . In this picture (Fig. 8), the results show that there is no such point in \bar{x} where both $\sqrt{Re}C_{f_1}$ and $\sqrt{Re}C_{f_2}$ approaches 0 simultaneously. So, there is an ordinary separation exists but no singular separation

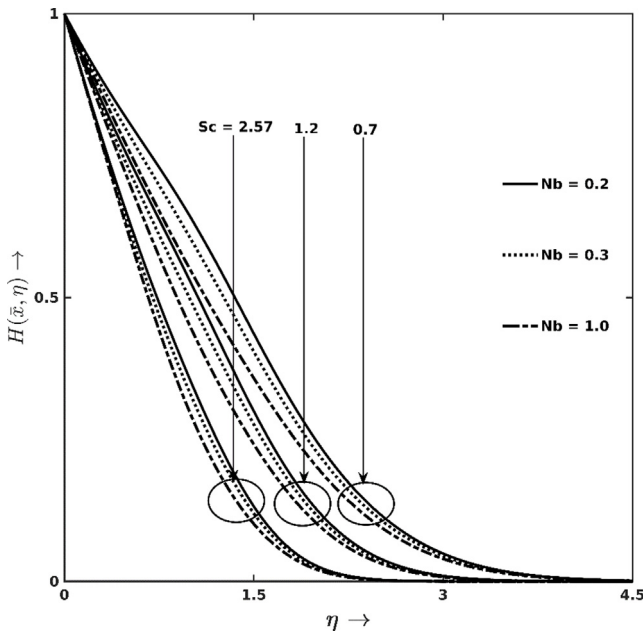


Fig. 7 Nb and Sc variation against H.

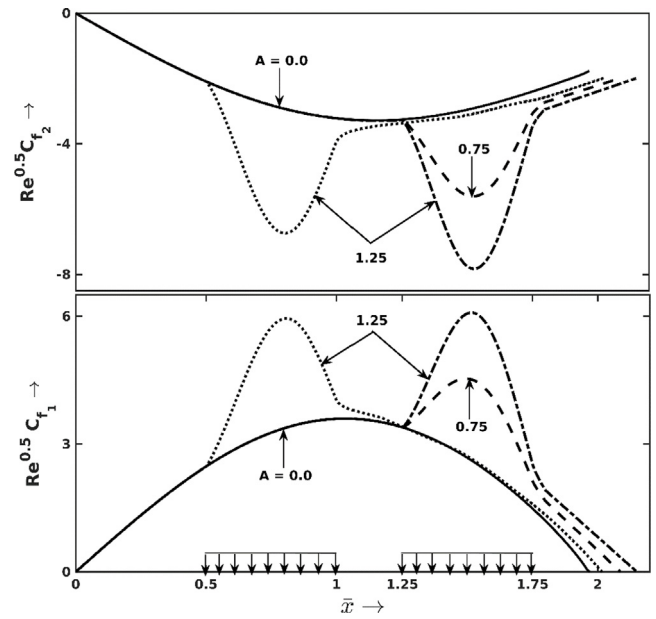


Fig. 9 Effects of A and \bar{x} on the friction coefficients $\sqrt{Re}C_{f_1}$ and $\sqrt{Re}C_{f_2}$.

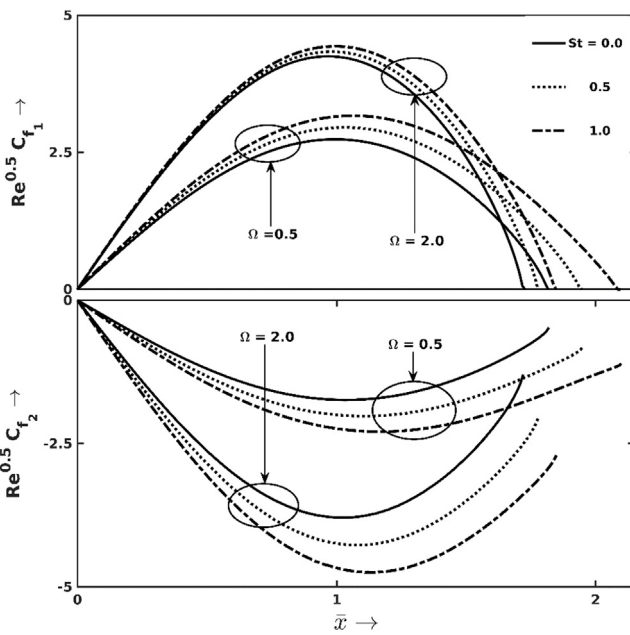


Fig. 8 Effects of St and Ω on friction coefficients $\sqrt{Re}C_{f_1}$ and $\sqrt{Re}C_{f_2}$.

exists. The details on different types of separations are available on the referred texts [5]. As it has been brought into notice earlier that the flow intensity F increases with Ω , hence the corresponding friction $\sqrt{Re}C_{f_1}$ gets augmented for heightening Ω and the exact opposite trend takes place for the other friction component $\sqrt{Re}C_{f_2}$. Moreover, due to higher Ω , the pressure transformed into kinetic energy for the high speed flows (in x direction) in the first half of the sphere, though in the second half, the fluid particles adjacent to the surface loses most of their kinetic energies and separates early in the flow due to high pressure ahead. Contradictorily, the zero friction point

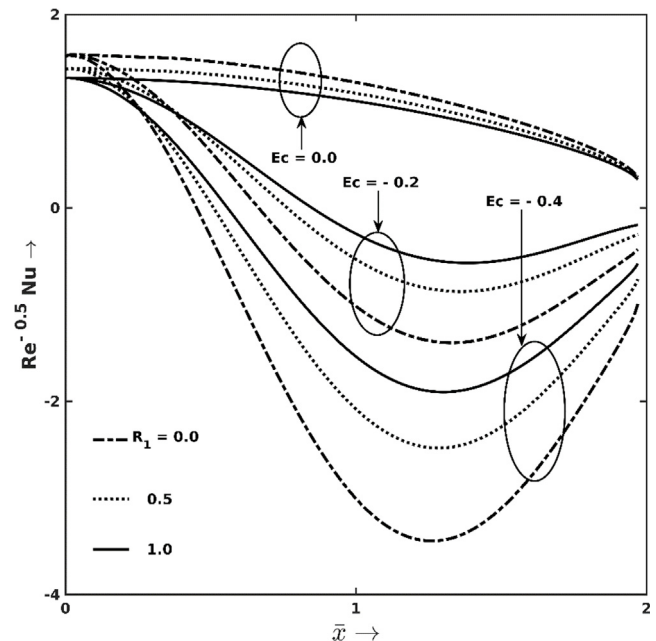


Fig. 10 Effects of Ec and R_1 on the thermal transport coefficient $\frac{Nu}{\sqrt{Re}}$.

(i.e., the separation point) pushes downstream for augmented values of St . The numerical scrutiny summarizes that the flow separates at $\eta = 1.945$ for $\Omega = 0.5$ whereas the same happens at $\eta = 1.78$ for $\Omega = 2.0$ keeping fixed $St = 0.5$.

The impacts of slot suction with its position (\bar{x}), and strengths (A) on the friction coefficients $\sqrt{Re}C_{f_1}$ and $\sqrt{Re}C_{f_2}$ are characterized graphically in Fig. 9. Visual inspection on Fig. 9 indicates that the zero friction position (i.e., the separation point) can be pushed downstream appointing a slot suction. In addition, enhancing the suction strength A as well as placing it at the downstream location, the separation can be

delayed further. The fluid at the proximity of bounding surface loses most of its kinetic energies fighting against the accumulated pressure near the separation point. In this scenario, suction in downstream takes away the retarded fluids from the bounding surface and the remaining fluids experience an extra push to move faster. Particularly, the separation takes place at 2.0159 for implementing a slot (suction) of magnitude $A = 1.25$ at $\bar{x} = 0.5$ while it happens at 2.150 if the slot is placed at $\bar{x} = 1.25$. Contradicting to this, slot injection has exactly opposite role on $\sqrt{Re}C_{f1}$ and $\sqrt{Re}C_{f2}$ but the figures are not present here to brief the manuscript.

The characterization of the coefficient of thermal transport $\frac{Nu}{\sqrt{Re}}$ affected by the radiation intensity (R_1) and dissipation (viscous) parameter Ec is portrayed in Fig. 10. The results proclaimed that $\frac{Nu}{\sqrt{Re}}$ drastically decreases for decreasing Ec values. Decrement in Ec magnitude physically interpret enhancement in viscous dissipation in this case. Further, due to the enhanced dissipative force (i.e., for higher $|Ec|$), the HNFs in the surface proximity heated up, sometimes become hotter than the hot wall. Thus, the desired procedure of heat convection from hot surface to the cooler freestream fluid gets disturbed and the transport coefficient $\frac{Nu}{\sqrt{Re}}$ shows negative magnitude. In fact, in such a scenario, instead of cooled down, the wall becomes hotter absorbing heat from neighbouring heated fluids. In addition, Fig. 10 purports the contradictory behaviour of $\frac{Nu}{\sqrt{Re}}$ under R_1 effects. Under enlarging R_1 effects, the coefficient $\frac{Nu}{\sqrt{Re}}$ deteriorates for $Ec = 0$ but improves for $Ec < 0$. At the instant $\bar{x} = 0.5$, with fixed $R_1 = 0.5$, changing Ec in the range $[0, -0.2]$ shows 49% decrement in $\frac{Nu}{\sqrt{Re}}$.

The changes in characteristic thermal transport coefficient and mass transport coefficient affected by slot-wise mass suction are presented in Fig. 11. As one can see, both $\frac{Nu}{\sqrt{Re}}$ and $\frac{Sh}{\sqrt{Re}}$ increase for strengthening the suction. As discussed earlier, the suction improves the flow intensity and correspondingly the gradients for mass and heat increase resulting enhancement in $\frac{Nu}{\sqrt{Re}}$ and $\frac{Sh}{\sqrt{Re}}$.

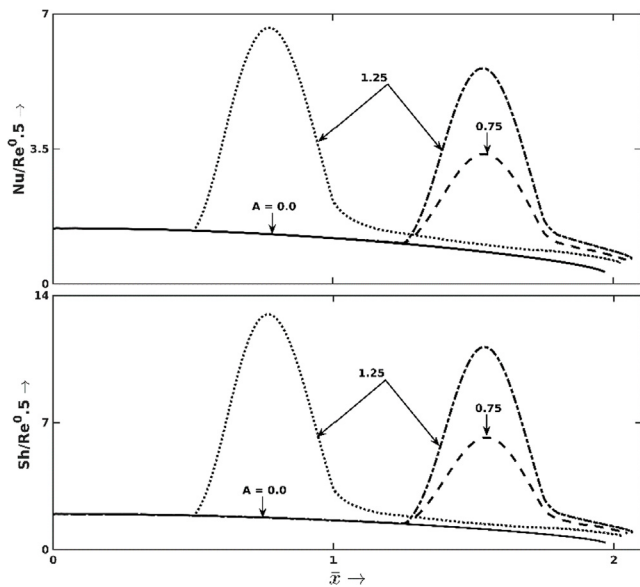


Fig. 11 Effects of A and \bar{x} on the transport coefficient $\frac{Nu}{\sqrt{Re}}$ and $\frac{Sh}{\sqrt{Re}}$.

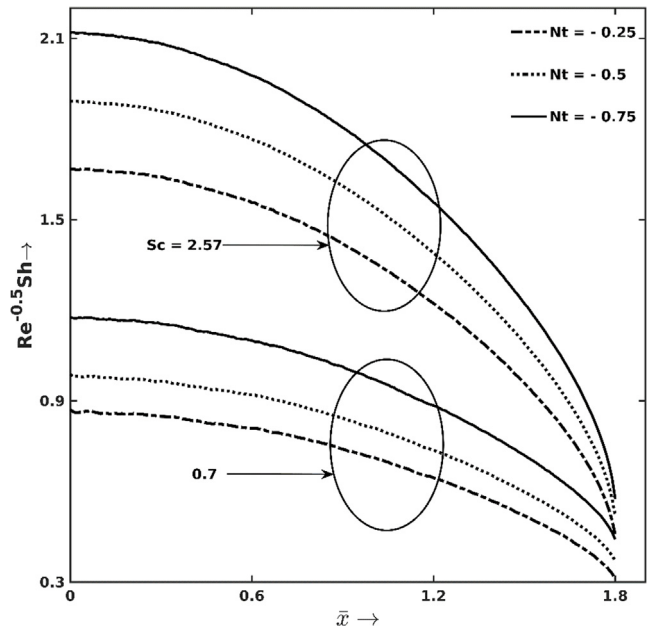


Fig. 12 Effects of Nt and Sc on the mass transport coefficient $\frac{Sh}{\sqrt{Re}}$.

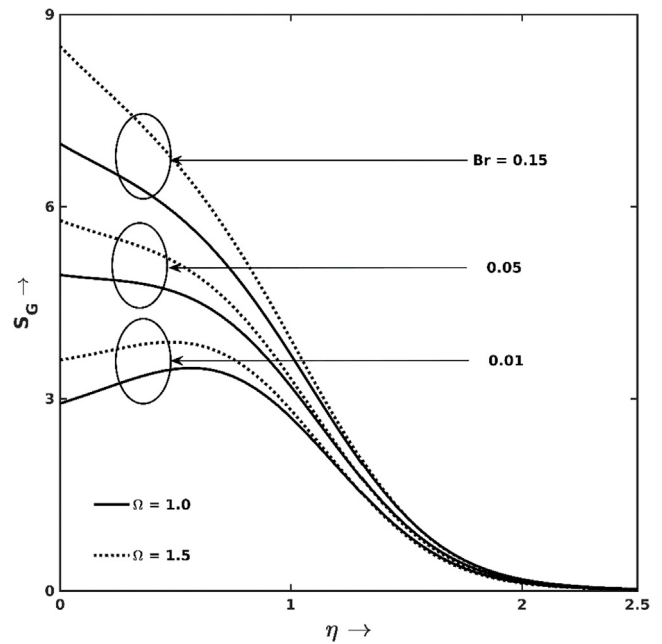


Fig. 13 Effects of Br and Ω on entropy production S_G .

The physical significance of diffusion parameters Nt (Thermophoresis) and Schmidt number Sc on mass transport coefficient $\frac{Sh}{\sqrt{Re}}$ are shown in Fig. 12 and it depicts descending tendency of $\frac{Sh}{\sqrt{Re}}$ for increasing estimations of Nt and Sc . The discussion in the earlier sections demonstrated that enlarging magnitudes of Sc declines the HNF concentration that reduces mass density. Correspondingly, the concerning mass gradient and hence the mass transfer rate $\frac{Sh}{\sqrt{Re}}$ increases. Further, Nt , the thermophoresis strength also elevates the mass transfer by migrating the hybrid NPs from hot wall to cooler

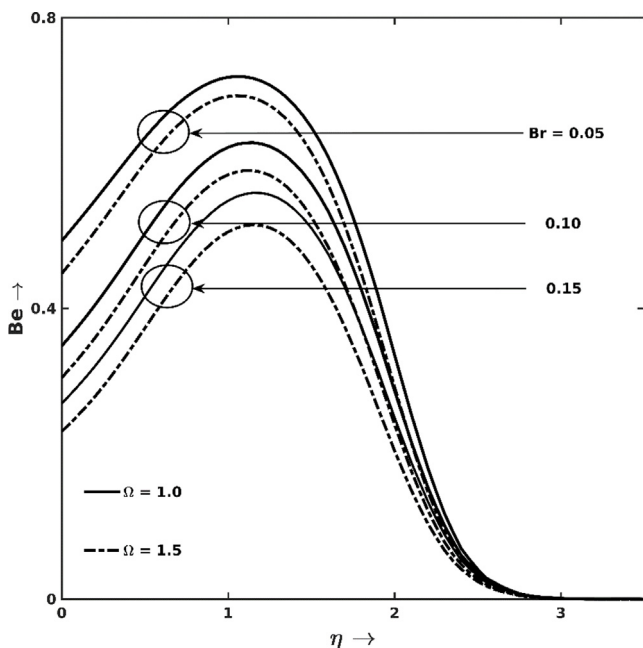


Fig. 14 Effects of Br and Ω on Bejan number Be .

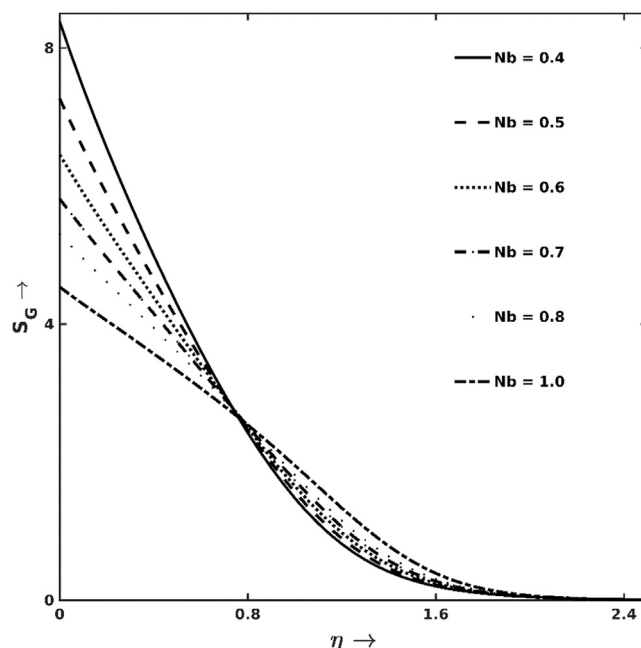


Fig. 16 Effects of Nb on entropy production S_G .

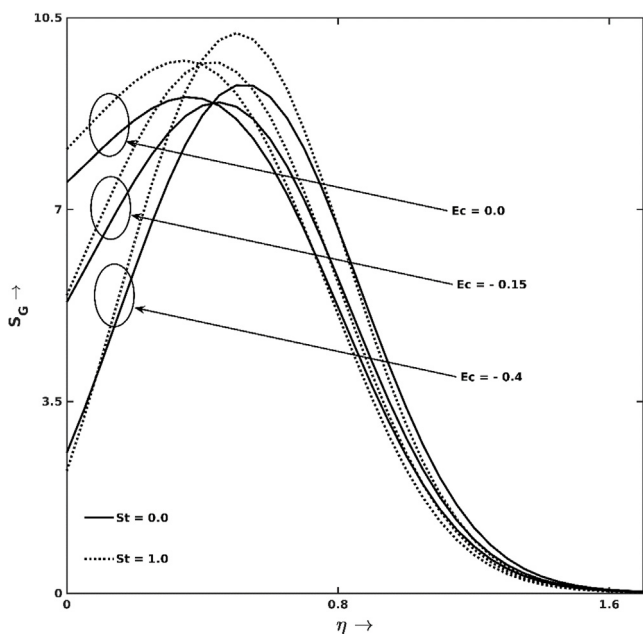


Fig. 15 Effects of Ec and St on entropy production S_G .

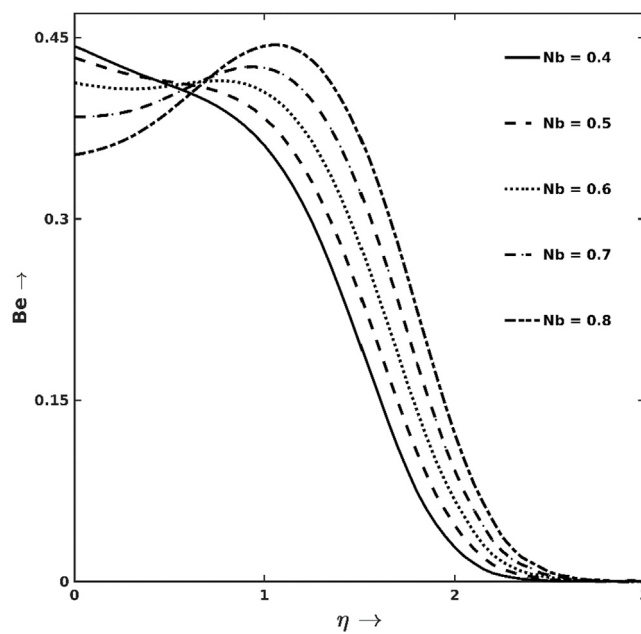


Fig. 17 Effects of Nb on Bejan number Be .

freestream region. Specific enumerations at $\bar{x} = 1.0$ with $Nt = -0.5$ show that $\frac{Sh}{\sqrt{Re}}$ enhances nearly by 90% for the enlargement of Sc from 0.7 to 2.57.

The bearings of entropy productions (S_G) and Bejan lines (Be) concerning to Br and Ω (viscous heating and rotation parameters, respectively) are displayed in Figs. 13–14. An inspection on the visual evidence (Fig. 13) reveals that S_G increases simultaneously with both Br and Ω . Higher estimations of Br physically represent more heat production due to friction between fluid layers in the BL region. Likewise, incremental estimations in rotation (Ω) enhances frictional heating

by strengthening the flow intensities. In either case, the degree of disorder increases immensely owing to frictional heating. In addition to these, the effects of both Br and Ω are predominantly observable at the wall proximity. The Bejan number graphs (Fig. 14) also affirm the same, the irreversibilities subject to friction (FFI) dominate over the sources (HTIs and DIs) at the neighbouring regions to the surface and as manifested in Fig. 14, the Bejan lines begin below for higher estimations of Br and Ω .

Fig. 15 is manifesting the entropy production rate S_G for various magnitudes of dissipation (Ec) and magnetic strengths

St . On closed observation, it is seen that S_G -production within the boundary layer but not adjacent to the surface for high magnitudes of Ec is high. Physically, a high-strength dissipative force generates adequate heat within the BL, even sometimes the fluids become hotter than the hot surface. In such cases, an enormous amount of heat loss consequences a high entropy production. Besides, a higher S_G -production is noticed for strengthening St .

The variations in entropy production rate (S_G) and Bejan number lines (Be) are drawn in Figs. 16 and 17, respectively, against the changes of Brownian (Nb) parameters. As depicted in Fig. 16, the strengthening of the Brownian parameter subsides it.

For a higher magnitude of Nb , the NPs move more haphazardly which helps the thermal convection and fluid within BL heated up. Hence the thermal gradient within the BL downgrades and the heat loss owing to HTI decreases. Further, for higher Nb , the increased haphazard NPs' motion makes the concentration BL homogeneous which reduces the concentration gradient and hence S_G -production for diffusion decreases. The Bejan lines are evidencing the same; for large Nb , initially, they stay down near the wall due to low levels of S_G -generation owing to HTI and DI , then gradually go up and then eventually converge to zero.

8. Conclusions

This study deals for a forced convective HNF flow under the limelight of temperature sensorial water properties (physical). The flow is considered over a complex geometric spinning sphere which has numerous practical implementations in engineering. The separation of BL from the surface is controlled via slot-wise mass disposal method. The flow is also considered under external radiation and magnetic effect. Further, this existing project is accomplished with modified Buongiorno model (MBM), the foremost advanced method available in literature. The governing PDEs (non-linear and coupled) have been solved employing sets of advanced numerical methods that comprised quasilinearization, finite difference (implicit), Vargas method. The following conclusive remarks are extracted and summarized in brief from the above detailed analysis:

- The flow intensity F accumulates for higher strengths of Ω and St while the other velocity component S subsides for the same.
- HNFs' temperature augmented for enlarging magnitudes of Ec and Nt that is the BL fluids' temperature increases for high intense viscous dissipation as well as for high thermophoretic diffusion
- The Schmidt number (Sc) and Brownian motion (Nb) negatively affect the concentration BL, the corresponding H -profile drops down for amplified values of Sc and Nb .
- The surface friction ($\sqrt{Re}C_{f_1}$) in meridional direction (\bar{x}) increases as the angular velocity (Ω) and strength of imposed magnetic field (St) increases. Although St pushes the separation downstream, Ω drags it to upstream.
- The separation point can be delayed remarkably employing slot-wise mass suction and the results are more fruitful for higher strengths slot suction positioned downstream. Results data shows nearly 6% and 10% delay in the

separation point for appointing a suction $A = 1.25$ and $A = 0.75$, respectively, at $\bar{x} = 1.25$.

- Heat transport performance drastically drops down for higher dissipation effect (Ec) but it gets surplus for R_1 and slot suction. Specifically, at $\bar{x} = 0.5$, $\frac{Nu}{\sqrt{Re}}$ downgrades almost by 97% for enriching Ec from 0.0 to -0.4 with fixed $R_1 = 0.5$.
- The surface mass transfer ($\frac{Sh}{\sqrt{Re}}$) remarkably elevates under enlarging estimations of thermophoresis (Nt) and Schmidt number (Sc).
- Entropy produces at a higher rate for Br and Ω but reduces significantly due to Brownian motion parameter (Nb).
- Entropy production (S_G) under dissipation (Ec) effect shows unfamiliar behaviour, it decreases at the surface and then increases instantly near the surface proximity for higher Ec .

Declaration of Competing Interest

The authors declare that they have no known competing financial interests or personal relationships that could have appeared to influence the work reported in this paper.

Appendix A.

$$D(\bar{x}) = \frac{T_3 T_5}{T_2}$$

$$D_{11} = N$$

$$D_{12} = -a_1 G_\eta N^2 + S_1 [f + 2D(\bar{x})f_{x^-}]$$

$$D_{13} = -2S_1 D(\bar{x})F$$

$$D_{14} = -S_1 \left[-2F \frac{T_3 T_4}{T_2} + 2D(\bar{x})F_{x^-} \right]$$

$$D_{15} = -a_1 F_\eta N^2$$

$$D_{16} = -a_1 F_{\eta\eta} N^2 + 2a_1^2 F_\eta G_\eta N^3$$

$$D_{17} = 2S_1 \frac{T_3 T_4}{T_2} \Omega S$$

$$D_{18} = 2a_1^2 F_\eta G_\eta G N^3 - a_1 F_{\eta\eta} G N^2 - S_1 \times \frac{T_3 T_4}{T_2} [(1 + F^2) + FF_{x^-} + \Omega S^2] - a_1 F_\eta G_\eta N^2 - \frac{4}{9} \times \frac{T_3}{T_2} K_1 St$$

$$D_{21} = N$$

$$D_{22} = -a_1 G_\eta N^2 + S_1 [f + 2D(\bar{x})f_{x^-}]$$

$$D_{23} = -2S_1 D(\bar{x})F$$

$$D_{24} = -2S_1 \frac{T_3 T_4}{T_2} F$$

$$D_{25} = -2S_1 \left[\frac{T_3 T_4}{T_2^2} - D(\bar{x}) S_{x^-} \right]$$

$$D_{26} = -a_1 S_\eta N^2$$

$$D_{27} = -a_1 S_{\eta\eta} N^2 + 2a_1^2 S_\eta G_\eta N^3$$

$$D_{28} = 2a_1^2 S_\eta G_\eta G N^3 - 2S_1 \left[\frac{T_3 T_4}{T_2^2} S F - D(\bar{x}) S_{x^-} F \right] - a_1 S_\eta G_\eta N^2 - a_1 S_{\eta\eta} G N^2$$

$$D_{31} = \frac{N}{Pr} [P_5 + R_1]$$

$$D_{32} = 2G_\eta \left[P_5 P_6 + \frac{N}{Pr} P_7 \right] + S_2 (f + 2D(\bar{x}) f_{x^-}) + (2G_\eta N t + N b H_\eta)$$

$$D_{33} = -S_2 D(\bar{x}) F$$

$$D_{34} = G_{\eta\eta} \left[P_6 (P_5 + R_1) + \frac{N}{Pr} P_7 \right] + G_\eta^2 \left[2P_6 P_7 + P_5 P_8 + \frac{N}{Pr} P_9 \right] + \frac{9}{4} \frac{a_1 E c N^2}{(1-\phi)^{2.5}} T_1 T_2 \left[F_\eta^2 + \Omega S_\eta^2 \right]$$

$$D_{35} = \frac{9}{4} \frac{E c N}{(1-\phi)^{2.5}} T_1 T_2 [2F_\eta]$$

$$D_{36} = -2S_2 D(\bar{x}) G_{x^-}$$

$$D_{37} = \frac{9}{4} \frac{E c N}{(1-\phi)^{2.5}} T_1 T_2 [2\Omega S_\eta]$$

$$D_{38} = N b G_\eta$$

$$D_{39} = G G_{\eta\eta} \left[(P_5 + R_1) P_6 + \frac{N}{Pr} P_7 \right] + G_\eta^2 \left[P_5 P_6 + \frac{N}{Pr} P_7 \right] + G G_\eta^2 \left[2P_6 P_7 + P_5 P_8 + \frac{N}{Pr} P_9 \right]$$

$$-2S_2 D(\bar{x}) F G_{x^-} + (N b H_\eta G_\eta + N t G_\eta^2) + \frac{9}{4} \frac{a_2 E c N^2}{(1-\phi)^{2.5}} T_1 T_2 \left[F_\eta^2 + \Omega S_\eta^2 \right]$$

$$D_{41} = 1$$

$$D_{42} = S c [f + 2D(\bar{x}) f_{x^-}]$$

$$D_{43} = -2S c D(\bar{x}) F$$

$$D_{44} = -2S c D(\bar{x}) H_{x^-}$$

$$D_{45} = \frac{N t}{N b}$$

$$D_{46} = -2S c D(\bar{x}) F H_{x^-}$$

References

- [1] M. Kumari, G. Nath, Nonsimilar laminar incompressible boundary layer flow over a rotating sphere, *Arch. Mech., Archiwum Mechaniki Stosowanej*. 34 (2) (1982) 147–164.
- [2] M. Kumari, G. Nath, Unsteady Incompressible Boundary-Layer Flow Over a Rotating Sphere, *J. Appl. Mech.* 49 (1) (1982) 234–236.
- [3] H.S. Takhar, A. Slaouti, M. Kumari, G. Nath, Unsteady free convection flow in the stagnation-point region of a rotating sphere, *Int. J. Non Linear Mech.* 33 (5) (1998) 857–865.
- [4] P. Saikrishnan, S. Roy, Steady nonsimilar axisymmetric water boundary layers with variable viscosity and Prandtl number, *Acta Mech.* 157 (1) (2002) 187–199.
- [5] S. Roy, P. Saikrishnan, Non-uniform slot injection (suction) into steady laminar water boundary layer flow over a rotating sphere, *Int. J. Heat Mass Transf.* 46 (18) (2003) 3389–3396.
- [6] M. Turkyilmazoglu, Numerical and analytical solutions for the flow and heat transfer near the equator of an MHD boundary layer over a porous rotating sphere, *Int. J. Therm. Sci.* 50 (5) (2011) 831–842.
- [7] A. Mahdy, A. Mahdy, A.J. Chamkha, H.A. Nabwey, Entropy analysis and unsteady MHD mixed convection stagnation-point flow of Casson nanofluid around a rotating sphere, *Ale, Eng. J.* 59 (3) (2020) 1693–1703.
- [8] A. Malvandi, The unsteady flow of a nanofluid in the stagnation point region of a time-dependent rotating sphere, *Therm. Sci.* 19 (5) (2015) 1603–1612.
- [9] P.M. Patil, S. Benawadi, B. Shanker, Influence of mixed convection nanofluid flow over a rotating sphere in the presence of diffusion of liquid hydrogen and ammonia, *Math. Comput. Simul.* 194 (2022) 764–781.
- [10] T. Gul, B. Ali, W. Alghamdi, S. Nasir, A. Saeed, P. Kumam, S. Mukhtar, W. Kumam, M. Jawad, Mixed convection stagnation point flow of the blood based hybrid nanofluid around a rotating sphere, *Sci. Rep.* 11 (1) (2021) 1–5.
- [11] M.M. Usman, A. Bhatti, M.H.D. Ghaffari, The role of radiation and bioconvection as an external agent to control the temperature and motion of fluid over the radially spinning circular surface: A theoretical analysis via Chebyshev spectral approach, *Math. Meth. Appl. Sci.* (2022) 1–18, <https://doi.org/10.1002/mma.8085>.
- [12] S.U. Khan, Usman, K. Al-Khaled, S.M. Hussain, A. Ghaffari A, M.I. Khan, M.W. Ahmed, Implication of Arrhenius activation energy and temperature-dependent viscosity on non-Newtonian nanomaterial bio-convective flow with partial slip, *Arab. J. Sci. Eng.* 47(6) (2022) 7559–70.
- [13] S.A. Alsallami, S.U. Usman, A. Khan, M.I. Ghaffari, M.A. Khan, M.R.K. El-Shorbagy, Numerical simulations for optimised flow of second-grade nanofluid due to rotating disk with nonlinear thermal radiation: Chebyshev spectral collocation method analysis, *Pramana–J, Phys.* 96 (2) (2022) 98.
- [14] P. Usman, A. Lin, Ghaffari, Heat and mass transfer in a steady flow of Sutterby nanofluid over the surface of a stretching wedge, *Phys. Scr.* 96 (6) (2021) 065003.
- [15] M. Ghalambaz, A. Doostani, E. Izadpanahi, A.J. Chamkha, Conjugate natural convection flow of Ag–MgO/water hybrid nanofluid in a square cavity, *J. Therm. Anal. Calorim.* 139 (3) (2020) 2321–2336.
- [16] A.M. Rashad, A.J. Chamkha, M.A. Ismael, T. Salah, Magneto-hydrodynamics natural convection in a triangular cavity filled with a Cu–Al₂O₃/water hybrid nanofluid with localized heating from below and internal heat generation, *J. Heat Transf.* 140 (7) (2018) 072502.
- [17] A.I. Alsabery, T. Tayebi, H.T. Kadhim, M. Ghalambaz, I. Hashim, A.J. Chamkha, Impact of two-phase hybrid nanofluid

- approach on mixed convection inside wavy lid-driven cavity having localized solid block, *J. Adv. Res.* 30 (2021) 63–74.
- [18] M.A. Ismael, T. Armaghani, A.J. Chamkha, Mixed convection and entropy generation in a lid-driven cavity filled with a hybrid nanofluid and heated by a triangular solid, *Heat Transf. Res.* 49 (17) (2018) 1645–1665.
- [19] M.M. Bhatti, S.I. Abdelsalam, Bio-inspired peristaltic propulsion of hybrid nanofluid flow with Tantalum (Ta) and Gold (Au) nanoparticles under magnetic effects, *Waves in Random and Complex Media.* 9 (2021) 1–26.
- [20] M.M. Bhatti, H.F. Öztöp, R. Ellahi, I.E. Sarris, M.H. Doranehgard, Insight into the investigation of diamond (C) and Silica (SiO₂) nanoparticles suspended in water-based hybrid nanofluid with application in solar collector, *J. Mol. Liq.* 357 (2022) 119134.
- [21] L. Zhang, M.M. Bhatti, E.E. Michaelides, M. Marin, R. Ellahi, Hybrid nanofluid flow towards an elastic surface with tantalum and nickel nanoparticles, under the influence of an induced magnetic field, *Eur. Phys. J. Spec. Top.* 231 (3) (2022) 521–533.
- [22] F. Wang, U. Nazir, M. Sohail, E.R. El-Zahar, C. Park, P. Thounthong, A Galerkin strategy for tri-hybridized mixture in ethylene glycol comprising variable diffusion and thermal conductivity using non-Fourier's theory, *Nanotechnol. Rev.* 11 (1) (2022) 834–845.
- [23] U. Nazir, M. Sohail, M.M. Selim, H. Alrabaiah, P. Kumam, Finite element simulations of hybrid nano-Carreau Yasuda fluid with hall and ion slip forces over rotating heated porous cone, *Sci. Rep.* 11 (1) (2021) 1–5.
- [24] E.A. Algehyne, E.R. El-Zahar, S.H. Elhag, F.S. Bayones, U. Nazir, M. Sohail, P. Kumam, Investigation of thermal performance of Maxwell hybrid nanofluid boundary value problem in vertical porous surface via finite element approach, *Sci. Rep.* 12 (1) (2022) 1–2.
- [25] J. Buongiorno, Convective transport in nanofluids, *ASME J. Heat Transfer.* 128 (2006) 240–250.
- [26] B. Mahanthesh, S.A. Shehzad, J. Mackolil, N.S. Shashikumar, Heat transfer optimization of hybrid nanomaterial using modified Buongiorno model: A sensitivity analysis, *Int. J. Heat Mass Transf.* 171 (2021) 121081.
- [27] V. Puneeth, R. Anandika, S. Manjunatha, M.I. Khan, M.I. Khan, A. Althobaiti, A.M. Galal, Implementation of modified Buongiorno's model for the investigation of chemically reacting rGO-Fe₃O₄-TiO₂-H₂O ternary nanofluid jet flow in the presence of bio-active mixers, *Chem. Phys. Lett.* 786 (2022) 139194.
- [28] P. Rana, N. Srikantha, T. Muhammad, G. Gupta, Computational study of three-dimensional flow and heat transfer of 25 nm Cu-H₂O nanoliquid with convective thermal condition and radiative heat flux using modified Buongiorno model, *Case Stud. Therm. Eng.* 27 (2021) 101340.
- [29] W. Owhaib, M. Basavarajappa, W. Al-Kouz, Radiation effects on 3D rotating flow of Cu-water nanoliquid with viscous heating and prescribed heat flux using modified Buongiorno model, *Sci. Rep.* 11 (2021) 1–6.
- [30] V. Puneeth, S. Manjunatha, J.K. Madhukesh, G.K. Ramesh, Three dimensional mixed convection flow of hybrid casson nanofluid past a non-linear stretching surface: A modified Buongiorno's model aspects, *Chaos Solitons Fractals.* 152 (2021) 111428.
- [31] G.K. Ramesh, A.J. Chamkha, B.J. Gireesha, MHD mixed convection flow of a viscoelastic fluid over an inclined surface with a nonuniform heat source/sink, *Can. J. Phys.* 91 (2013) 1074–1080.
- [32] W. Alghamdi, A. Alsubie, P. Kumam, A. Saeed, T. Gul, MHD hybrid nanofluid flow comprising the medication through a blood artery, *Sci. Rep.* 11 (1) (2021) 1–3.
- [33] K. Anantha Kumar, N. Sandeep, V. Sugunamma, I.L. Animasaun, Effect of irregular heat source/sink on the radiative thin film flow of MHD hybrid ferrofluid, *J. Therm. Anal. Calorim.* 139 (3) (2020) 2145–2153.
- [34] M.N. Othman, A. Jedi, N.A. Bakar, MHD flow and heat transfer of hybrid nanofluid over an exponentially shrinking surface with heat source/sink, *Appl. Sci.* 11 (17) (2021) 8199.
- [35] M. Shoaib, M.A. Raja, M.T. Sabir, S. Islam, Z. Shah, P. Kumam, H. Alrabaiah, Numerical investigation for rotating flow of MHD hybrid nanofluid with thermal radiation over a stretching sheet, *Sci. Rep.* 10 (1) (2020) 1–5.
- [36] A.I. Alsabery, M. Ghalambaz, T. Armaghani, A.J. Chamkha, I. Hashim, M. Saffari Pour, Role of rotating cylinder toward mixed convection inside a wavy heated cavity via two-phase nanofluid concept, *Nanomaterials* 10 (6) (2020) 1138.
- [37] P.B.A. Reddy, Biomedical aspects of entropy generation on electromagnetohydrodynamic blood flow of hybrid nanofluid with nonlinear thermal radiation and non-uniform heat source/sink, *Eur. Phys. J. Plus.* 135 (10) (2020) 1–30.
- [38] M. Shoaib, M.A. Raja, M.T. Sabir, M. Awais, S. Islam, Z. Shah, P. Kumam, Numerical analysis of 3-D MHD hybrid nanofluid over a rotational disk in presence of thermal radiation with Joule heating and viscous dissipation effects using Lobatto IIIA technique, *Alex. Eng. J.* 60 (4) (2021) 3605–3619.
- [39] P. Usman, A. Lin, Ghaffari, Steady flow and heat transfer of the power-law fluid between two stretchable rotating disks with non-uniform heat source/sink, *J. Therm. Anal. Calorim.* 146 (2021) 1735–1749.
- [40] T. Naseem, U. Nazir, M. Sohail, H. Alrabaiah, E.S. Sherif, C. Park, Numerical exploration of thermal transport in water-based nanoparticles: A computational strategy, *Case Stud. Therm. Eng.* 27 (2021) 101334.
- [41] S. Bilal, M. Sohail, R. Naz, Heat transport in the convective Casson fluid flow with homogeneous-heterogeneous reactions in Darcy-Forchheimer medium, *Multidiscip. Model. Mater. Struct.* 15 (6) (2019), 10.0.4.84/MMMS-11-2018-0202.
- [42] M. Yasin, S. Hina, R. Naz, T. Abdeljawad, M. Sohail, Numerical Examination on Impact of Hall Current on Peristaltic Flow of Eyring-Powell Fluid under Ohmic-Thermal Effect with Slip Conditions, *Curr. Nanosci.* 19 (1) (2023) 49–62.
- [43] M.I. Khan, M.U. Hafeez, T. Hayat, M.I. Khan, A. Alsaedi, Magneto rotating flow of hybrid nanofluid with entropy generation, *Comput. Methods Programs Biomed.* 183 (2020) 105093.
- [44] M.Z. Qureshi, S. Bilal, M.B. Ameen, T. Mushtaq, M.Y. Malik, Numerical examination about entropy generation in magnetically effected hybridized nanofluid flow between orthogonal coaxial porous disks with radiation aspects, *Surf. Interfaces.* 26 (2021) 101340.
- [45] Y.X. Li, M.I. Khan, R.P. Gowda, A. Ali, S. Farooq, Y.M. Chu, S.U. Khan, Dynamics of aluminum oxide and copper hybrid nanofluid in nonlinear mixed Marangoni convective flow with entropy generation: Applications to renewable energy, *Chinese, J. Phys.* 73 (2021) 275–287.
- [46] T.A. Yusuf, F. Mabood, W.A. Khan, J.A. Gbadeyan, Irreversibility analysis of Cu-TiO₂-H₂O hybrid-nanofluid impinging on a 3-D stretching sheet in a porous medium with nonlinear radiation: Darcy-Forchheimer's model, *Alex. Eng. J.* 59 (6) (2020) 5247–5261.
- [47] A.S. Dogonchi, S.R. Mishra, A.J. Chamkha, M. Ghodrati, Y. Elmasry, H. Alhumade, Thermal and entropy analyses on buoyancy-driven flow of nanofluid inside a porous enclosure with two square cylinders: Finite element method, *Case Stud. Therm. Eng.* 27 (2021) 101298.
- [48] P.B.A. Reddy, T. Salah, S. Jakeer, M.A. Mansour, A.M. Rashad, Entropy generation due to magneto-natural convection in a square enclosure with heated corners saturated porous medium using Cu/water nanofluid, *Chinese, J. Phys.* 77 (2022) 1863–1884.

- [49] A. Usman, I. Ghaffari, T.M. Mustafa, Y. Altaf, Analysis of entropy generation in a power-law nanofluid flow over a stretchable rotatory porous disk, *Case Stud. Therm. Eng.* 28 (2021) 101370.
- [50] Y.M. Li, K. Al-Khaled, S. Gouadria, E.R. El-Zahar, S.U. Usman, M.I. Khan, M.Y.M. Khan, Numerical simulations for three-dimensional rotating porous disk flow of viscoelastic nanomaterial with activation energy, heat generation and Nield boundary conditions, *Waves Random Complex Media.* 32 (6) (2022) 1–20.
- [51] R. Naz, S. Tariq, M. Sohail, Z. Shah, Investigation of entropy generation in stratified MHD Carreau nanofluid with gyrotactic microorganisms under Von Neumann similarity transformations, *Eur. Phys. J. Plus.* 135 (2) (2020) 1–22.
- [52] D.R. Lide (Ed.), *CRC Handbook of Chemistry and Physics*, CRC Press, 2004 Jun 29.
- [53] R.S. Varga, *Matrix Iterative Analysis, Second Revised and Expanded ed.*, Springer-Verlag, New York, Berlin, Heidelberg, Springer; 2000.
- [54] G. Revathi, P. Saikrishnan, A.J. Chamkha, Non-similar solutions for unsteady flow over a yawed cylinder with non-uniform mass transfer through a slot, *Ain Shams Eng. J.* 5 (4) (2014) 1199–1206.
- [55] T. Salahuddin, N. Siddique, M. Khan, Y.M. Chu, A hybrid nanofluid flow near a highly magnetized heated wavy cylinder, *Alex. Eng. J.* 61 (2) (2022) 1297–1308.
- [56] T. Barman, S. Roy, A.J. Chamkha, A Bi-Convective Magnetized Hybrid Nanofluid Flow Along with Thermal Radiation in an Adverse Pressure Field Using Temperature-Sensitive Base Fluid (Water) Properties, *J. Nanofluids* 11 (1) (2022) 142–153.
- [57] A.A. Usman, H. Memon, T. Anwaar, A.A. Muhammad, A.S. Alharbi, Y.R. Alshomrani, Aladwani, A forced convection of water-aluminum oxide nanofluids in a square cavity containing a circular rotating disk of unit speed with high Reynolds number: A Comsol Multiphysics study, *Case Stud. Therm. Eng.* 39 (2022) 102370.
- [58] H. Schlichting, K. Gersten, *Boundary Layer Theory*, Springer Science & Business Media, New York, 2003.